nature geoscience

ARTICLES

PUBLISHED ONLINE: 5 JUNE 2011 | DOI: 10.1038/NGEO1179

Slow release of fossil carbon during the Palaeocene–Eocene Thermal Maximum

Ying Cui[1]*, Lee R. Kump[1], Andy J. Ridgwell[2], Adam J. Charles[3], Christopher K. Junium[1†], Aaron F. Diefendorf[1†], Katherine H. Freeman[1], Nathan M. Urban[1†] and Ian C. Harding[3]

The transient global warming event known as the Palaeocene–Eocene Thermal Maximum occurred about 55.9 Myr ago. The warming was accompanied by a rapid shift in the isotopic signature of sedimentary carbonates, suggesting that the event was triggered by a massive release of carbon to the ocean–atmosphere system. However, the source, rate of emission and total amount of carbon involved remain poorly constrained. Here we use an expanded marine sedimentary section from Spitsbergen to reconstruct the carbon isotope excursion as recorded in marine organic matter. We find that the total magnitude of the carbon isotope excursion in the ocean–atmosphere system was about 4‰. We then force an Earth system model of intermediate complexity to conform to our isotope record, allowing us to generate a continuous estimate of the rate of carbon emissions to the atmosphere. Our simulations show that the peak rate of carbon addition was probably in the range of 0.3–1.7 Pg C yr^{-1}, much slower than the present rate of carbon emissions.

The Palaeocene–Eocene Thermal Maximum (PETM) was a geologically abrupt (~170,000-yr duration; ref. 1), extreme global warming event that occurred at about 55.9 million years ago (Myr; ref. 2). The main phase of the PETM was characterized by a ~5 °C global warming[3,4] driven by the massive release of greenhouse gas, as reflected in a contemporaneous negative carbon isotope excursion (CIE) in the ocean–atmosphere system[5]. Pervasive dissolution of deep sea sedimentary carbonate[6,7] indicates that either the source or its oxidation product was CO_2. Methane hydrate dissociation[8,9] and terrestrial or marine organic matter oxidation[10,11] may have amplified initial warming from volcanism-associated thermogenic gas release from sediments[12]; the comparative contributions from these sources determined the magnitude of the isotope excursion as well as the degree of warming and the extent of seafloor dissolution. The PETM was followed by an interval of rapid carbonate deposition on the sea floor[13], the expected response to a large carbon addition to the atmosphere that stimulates weathering delivering alkalinity to the ocean[14,15].

Core location and stratigraphic context

Upper Palaeocene and lower Eocene marine sediments were obtained from core BH9-05 (~77° 50′ N, 16° 30′ E) in the Palaeogene Central Basin of Spitsbergen[16] (Fig. 1a). The cored interval was deposited in a subsiding foreland basin associated with the West Spitsbergen Orogeny[17]. The lower Frysjaodden Formation (Fig. 1b) consists of organic-carbon-rich[18], laminated siliciclastic mudstones[19], barren of calcareous and siliceous microfossils but containing agglutinated foraminifera, organic-walled dinoflagellate cysts[2,20], pollen and spores, and terrestrial and marine biomarkers. High-resolution records of total organic carbon isotopes ($\delta^{13}C_{TOC}$) exhibit a prominent negative CIE of ~−4.2‰ from 536 to 519.7 m below surface (mbs), followed by a gradual concavo-convex shaped recovery (Fig. 2a). An orbital age model[2] constrained by a total PETM duration of ~170 kyr (ref. 2), indicates ~19 kyr for the onset of the event (from initiation to minimum $\delta^{13}C_{TOC}$).

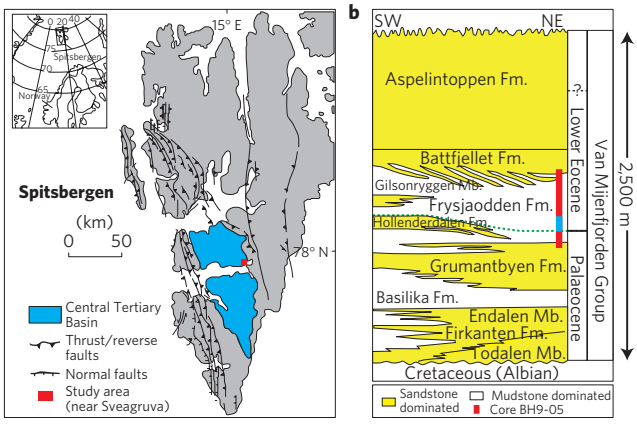

Figure 1 | Study area. a, Location map showing Palaeogene deposits in Spitsbergen. The red square represents the location of the study area near Sveagruva and Urdkollbreen. The drill core (BH9-05) site is located on the eastern margin of the Palaeogene Central Basin (77° 50′ N, 16° 30′ E). **b**, Stratigraphy of the Van Mijenfjorden Group (modified from refs 16 and 17). Core BH9-05 is shown as a red rectangle, which spans the Palaeocene/Eocene boundary. The geochemical and isotopic analyses in this study are from the blue highlighted interval.

Sources of sedimentary organic carbon

Because of the potential influence on $\delta^{13}C_{TOC}$ from different organic carbon sources, we evaluated evidence for source changes during

[1]Department of Geosciences, Pennsylvania State University, University Park, Pennsylvania 16802, USA, [2]School of Geographical Sciences, University of Bristol, University Road, Bristol BS8 1SS, UK, [3]School of Ocean and Earth Science, National Oceanography Centre Southampton, University of Southampton, European Way, Southampton SO14 3ZH, UK. †Present addresses: Department of Earth and Planetary Science, Northwestern University, Evanston, Illinois 60208, USA (C.K.J.); Department of Geology, University of Cincinnati, Cincinnati, Ohio 45221, USA (A.F.D.); Woodrow Wilson School of Public and International Affairs, Princeton University, Princeton, New Jersey 08544, USA (N.M.U.). *e-mail: yzc122@psu.edu; cuiying00@gmail.com.

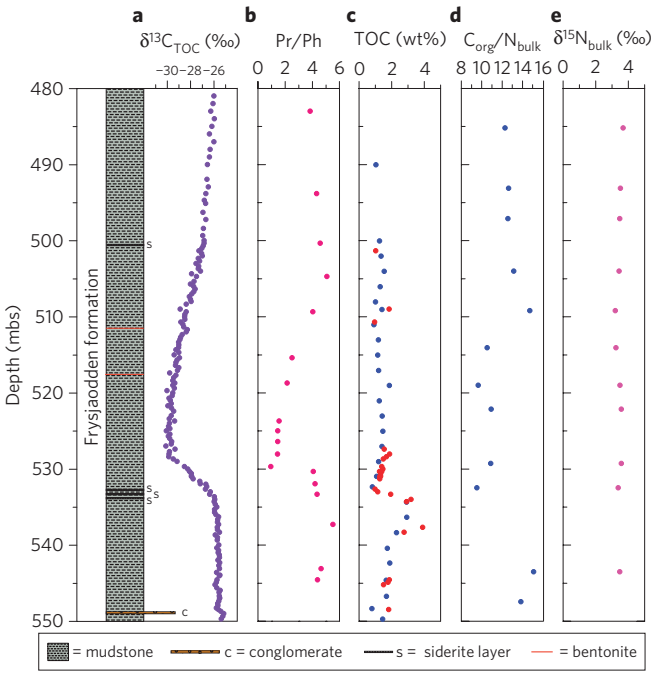

Figure 2 | Geochemical profiles throughout the PETM from core BH9-05 in Spitsbergen. a, Carbon isotopes of total organic carbon ($\delta^{13}C_{TOC}$). **b**, Pristane and phytane ratio denoted by Pr/Ph. **c**, Weight percentage of total organic carbon (wt% TOC), red dots are from this study, whereas blue dots are from ref. 18. **d**, C_{org}/N_{bulk} atomic ratio. **e**, $\delta^{15}N$ (‰) of bulk decarbonated sediment.

the PETM. Pristane to phytane ratios (Pr/Ph) decrease abruptly from >4 to ≤1 during the onset of the CIE (529.70 mbs; Fig. 2b), perhaps indicating a significant shift from a fluvially transported and terrestrially dominated organic material[21] to a more marine influenced source[22]. However, the drop in Pr/Ph ratio may also reflect developing anoxia during the presumed flooding event associated with the onset of the CIE (ref. 20), and this interpretation is consistent with well-developed lamination and abundant pyrite[18]. The large drop in Pr/Ph ratios is not accompanied by changes in the weight per cent of total organic carbon (wt% TOC), and $\delta^{13}C_{TOC}$ values change smoothly, without any indication of abrupt change in source composition (Fig. 2a). Instead, wt% TOC values increase before the CIE and then drop through the CIE (Fig. 2c). Lower wt% TOC values during the onset of the CIE may be the consequence of reduced rates of biological productivity; there is no clear evidence for a change in sedimentation rate that could explain this change (see Supplementary Figs S1, S2). With the development of anoxia in the basin (from 533 to 528 mbs), wt% TOC increases and the C_{org}/N_{bulk} ratio drops from 15 to 10 (Fig. 2d). However, the $\delta^{15}N$ of the bulk sediments shows no trend through the record (Fig. 2e), remaining between +3 and +4‰. The shifts in Pr/Ph and C_{org}/N_{bulk} could reflect a change in the source of organic matter, but could also be the result of diagenesis under more reducing conditions. In any event, the $\delta^{13}C_{TOC}$ record does not seem to be significantly influenced by changing organic matter source during the PETM.

We note that the rates of decline and overall variability in $\delta^{13}C_{TOC}$ during the onset of the CIE observed at core BH9-05 in Spitsbergen (Fig. 2a) are muted compared to the ones observed at, for example, the well-studied Maud Rise and Walvis Ridge locations (Supplementary Fig. S3). Temporary storage of terrestrial organic material in soils, lakes and floodplain deposits on land could tend to mix organic matter of various ages before it is transported and deposited in a terrestrially dominated foreland basin, smearing the isotopic record to an undetermined degree depending on soil organic matter residence times (see Supplementary Fig. S4 for a sensitivity analysis of this factor). However, the sediments we analysed were being shed from the rapidly uplifting West Spitsbergen orogen, a tectonic environment unlikely to have long residence-time soils; in small mountainous watersheds, aged organic matter is a small contributor to riverine particulate organic carbon[23]. However, streams draining such watersheds do carry unweathered fossil particulate organic matter[23]. The West Spitsbergen hinterland was composed of pre-Devonian basement rocks, late Palaeozoic carbonates, and Mesozoic shales and sandstones[24] that may have provided an indeterminate amount of fossil kerogen to the sediments. The effect of this input would be to dampen the magnitude of the CIE but not extend its apparent onset.

Quantifying the rate of carbon release

The EMIC (Earth system model of intermediate complexity) we use, GENIE, has been used in a previous study[25] to simulate the effect of a single pulse of CO_2 to the atmosphere. In that study, the carbon addition that generated a −4‰ excursion in 10 kyr and the best-fit to the observed extent of PETM seafloor $CaCO_3$ dissolution was 6,800 Pg of CO_2 with an isotopic composition of −22‰. Zeebe *et al.*[9] demonstrated with a box model that a rapid, 5 kyr pulse of CH_4 (with $\delta^{13}C = -50‰$) at a rate of ~0.6 Pg C yr^{-1} (for a total of 3,000 Pg C), followed by a prolonged 1,480 Pg C addition for about 50 kyr, fit the isotope data better than a single pulse and was consistent with the seafloor dissolution data, although the warming calculated by the model was insufficient.

Here, rather than specifying the carbon addition, we forced the EMIC to conform to the prescribed atmospheric $\delta^{13}C$ ($\delta^{13}C_{atm}$) record by adding carbon of a given isotopic composition (methane-derived CO_2, $\delta^{13}C = -60‰$ or organic matter-derived CO_2, $\delta^{13}C = -22‰$) to the atmosphere at each time step (See Methods for model description). We applied a tenth order polynomial fit to the $\delta^{13}C_{TOC}$ records from Spitsbergen to remove high frequency, possibly local variations, added 19.3‰ from the fitted $\delta^{13}C_{TOC}$ record to align it with an initial $\delta^{13}C$ value of −6.5‰ (Fig. 4a), and used this curve to force the atmosphere. Each simulation was of 170 kyr duration and took approximately a month of CPU time on the University of Bristol IWAN cluster. All the simulations were run twice, once with bioturbation in the sediments and once without, to assess the effect that loss of bioturbation would have on sediment wt% $CaCO_3$ (anticipating the need to invoke this to explain the South Atlantic/Walvis Ridge results, as in ref. 25).

Model-data comparison

We focus here on model-data comparisons from the two runs with the best model-data fit, one with an organic carbon source and a relatively high initial riverine alkalinity input that yielded higher seafloor carbonate content (that is, a relatively deep calcite compensation depth or CCD), referred to as the C_{org} simulation hereafter, and the other with a methane source and a somewhat lower alkalinity input and shallower initial CCD, referred to as the CH_4 simulation hereafter, both with bioturbation on (Supplementary Figs S5–S10 and Tables S1–S4).

The peak rate of carbon addition during the onset period is 0.3 Pg C yr^{-1} for CH_4 and 1.7 Pg C yr^{-1} for C_{org} (Fig. 4b), and in detail this peak rate is achieved in one of three pulses of carbon addition that occurred during the onset of the CIE. These rates have a linear dependence on our estimate of the duration of the onset based on an orbitally tuned age model for the core[2]. Our $\delta^{13}C_{TOC}$ record within this interval indicates the absence of unconformities on a scale that could bias age model interpretations (see Supplementary Information). The time-series used to derive the age model illustrate that one prominent

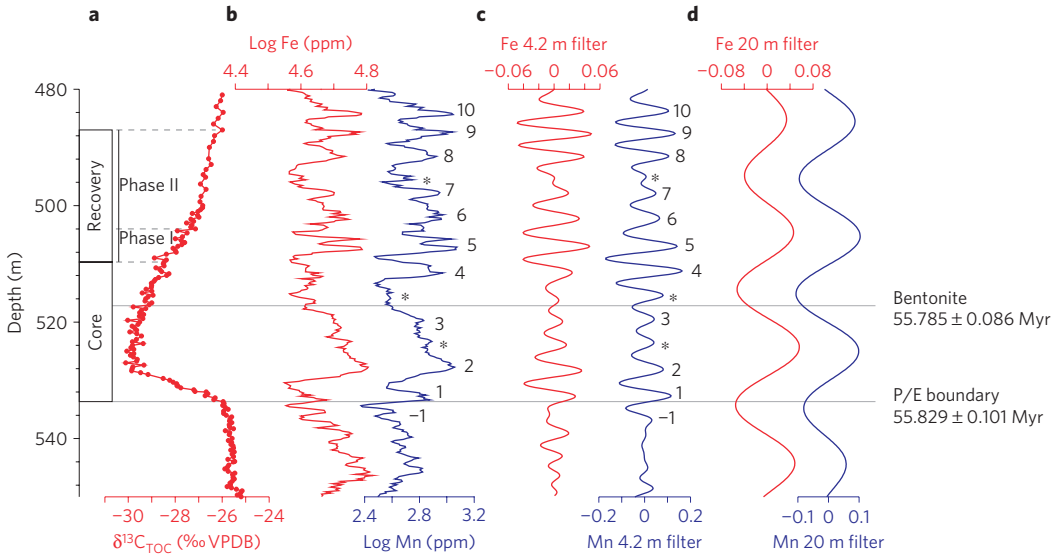

Figure 3 | Filtered records of core BH9-05 in the depth domain modified from ref. 2. a, $\delta^{13}C_{TOC}$ (‰) from this study. **b**, Core BH9-05 Log Fe (red) and Mn (blue) time series. **c**, Log Fe and Mn 4.2 m (0.24 ± 0.07 cycles m^{-1}) Gaussian filter output. Numbered cycles were interpreted as precession cycles and tuned to the Log Fe record from ODP Site 1263 (ref. 1) to derive the age model used in this study (Option A of ref. 2). **d**, Log Fe and Mn 20 m (0.05 ± 0.01 cycles m^{-1}) filter, inferred to represent the short (~100 kyr) component of orbital forcing.

cycle (labelled 1 in Fig. 3) is present within the onset interval (Fig. 3). Interpreted as a precession cycle[21], this indicates an apparent maximum duration of 21 kyr for the CIE onset (Fig. 3). Nevertheless, it is possible that this interval could have been shorter than a complete precession cycle. Therefore, we performed sensitivity analyses with a much more rapid pulse of carbon addition in the first 1 kyr, with half of the total carbon being injected, followed by 18 kyr of slow carbon injection such that in the end the total amount of carbon added was the same as in the original simulations. In these simulations the surface-water carbonate saturation states drop markedly (Supplementary Fig. S11), inconsistent with the lack of evidence for surface-water acidification during the PETM (ref. 26), and the pattern of CIE does not fit the observation (Supplementary Fig. S12). We also calculated peak isotope excursion rates (‰ per kyr) from other published isotope records with orbital or ^{3}He-based chronologies (Supplementary Fig. S13), because this rate of change reflects the rate of carbon addition during the onset interval. Most of these actually have longer durations for the onset interval and smaller peak rates of isotope change, and thus indicate peak carbon injection rates were significantly less than modern fossil-fuel burning rates (9 Pg C yr^{-1}; ref. 27), with the exception of the Site 690 simulations, which, because of one data point during the onset, have peak rates that may have exceeded our estimate by ~60% (still considerably less than the modern fossil-fuel burning rate; Supplementary Figs S3 and S13). Taken together, it seems likely that the rates we calculate here are reasonable estimates of the maximum rate of carbon release during the PETM. It is important in this context to note that the release of carbon seems to have come in at least three millennial-duration pulses, which in the model yield rates that exceed those that would result if the onset of the CIE was assumed to progress linearly to minimum value, as in previous work[25].

The total amount of carbon added to drive the isotope excursion (Fig. 4c) ranges from 2,500 (CH_4) to 13,000 Pg C (C_{org}). The model then requires an organic carbon burial event (extraction of ^{13}C-depleted material) during the early recovery phase of the CIE, as reflected by a substantial negative flux (~−0.5 Pg C yr^{-1} for C_{org}; Fig. 4b), followed by a 100-kyr interval of net organic carbon burial at slower rates (~−0.05 Pg C yr^{-1} for C_{org}; Fig. 4b). Apparently enhanced carbonate weathering in response to elevated atmospheric temperatures in the model was unable to restore the $\delta^{13}C$ of the surface ocean (and atmosphere) on a sufficiently fast timescale, consistent with a recent analysis of other PETM carbon isotope records[28]. Enhanced silicate weathering (a process not included in our simulations) can draw down atmospheric pCO_2 and neutralize ocean pH over tens to hundreds of thousands of years[14], but silicate weathering *per se* cannot change the isotopic composition of DIC of the ocean. The extraction of organic carbon explains why, by the end of the simulation, the total net addition of carbon is considerably less than that added during the onset of the CIE (Fig. 4c).

In our simulations, the atmospheric pCO_2 level is quite sensitive to the carbon source type but is indiscernibly affected by the pre-existing CCD and the effects of bioturbation (Supplementary Table S3). Atmospheric pCO_2 increases from 834 ppm to either 1,500 ppm (CH_4 scenario) or 4,200 ppm (C_{org} scenario) during the main phase of the PETM (Fig. 4d). The corresponding global ocean surface temperature increase during the peak PETM is ~2.1 °C (CH_4 scenario) and ~6.5 °C (C_{org} scenario) respectively (Fig. 4e). The model results for the CH_4 scenario are consistent with previous calculations of the effects of methane release during the PETM (refs 9,15). Although there is little proxy constraint on peak atmospheric CO_2 levels during the PETM, temperature is fairly well constrained, and the enhanced warming associated with the C_{org} scenario is more consistent with the observed degree of warming[3,4] than the CH_4 scenario assuming the methane is immediately converted to CO_2.

Discussion

We have two contrasting scenarios for the PETM, one with a small methane addition to an ocean with a relatively shallow initial CCD, and the other with a much larger CO_2 addition to an ocean with a somewhat deeper initial CCD. Unfortunately, the existing data constraints are insufficient to unambiguously discriminate between the scenarios. However, a deep initial CCD is a better fit to the pre-PETM condition, especially for Walvis Ridge and the South Indian/Southern Ocean (see Supplementary Information). The high sensitivity of the model to the pre-PETM buffering capacity of the ocean and sediments means that improved spatial coverage

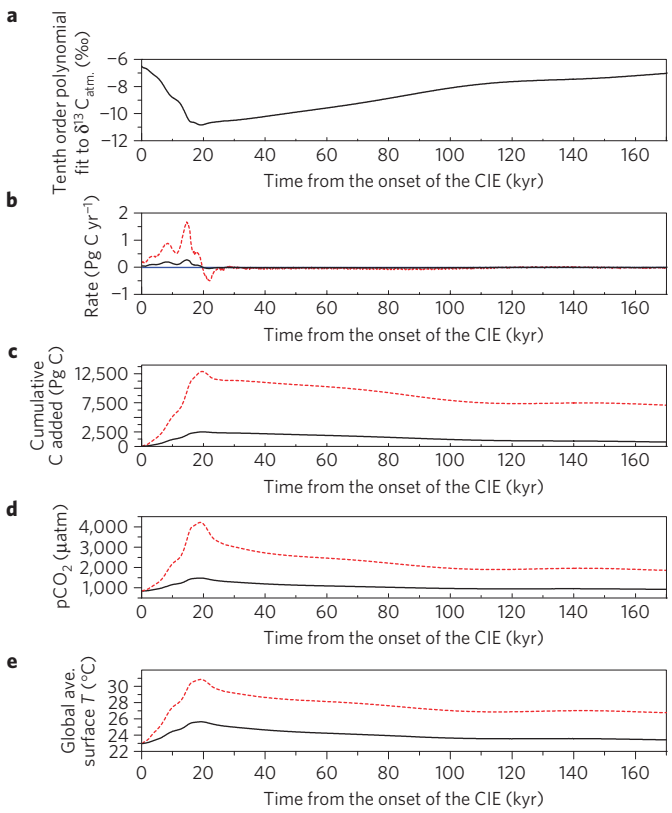

Figure 4 | Model results of the PETM carbon release rate and cumulative amount of carbon added versus time from the onset of the CIE (535 mbs) (age model is from ref. 2). a, $\delta^{13}C_{atm}$ that we used to force GENIE. **b**, Model results of the PETM carbon release rate. **c**, Model results of the cumulative amount of carbon added. **d**, Model results of the PETM atmospheric pCO_2. **e**, Model results of the PETM global average temperature (°C). The two best-fit simulations are shown in **b**–**e**:(1) CH_4 simulation (black solid line); (2) C_{org} simulation (red dotted line). Both simulations are with bioturbation on.

of the pre-PETM sedimentary record will one day resolve the issue of the source of carbon for the PETM.

Admittedly, the C_{org} scenario requires the release of quantities of CO_2 that greatly exceed estimates of the modern readily available carbon pools (in the form of biomass, soil carbon, and peat)[28] exclusive of seafloor methane hydrates. However, unlike the modern, the Late Palaeocene was a 'coal giant', that is, a rare interval in Earth history when abundant coal was deposited[10]. It is important to realize that 'C_{org}' here could actually represent a range of source types; all that is specified is its mean isotopic composition. It could be fossil organic matter (kerogen)[11] or peat/coal[10], but it could also be a mixture of isotopically heavier volcanic CO_2 (mantle-derived CO_2 with an isotopic composition of −5‰) and biogenic (−60‰) and/or thermogenic (−30‰) methane[12,29] and the dissociation of methane hydrates[8]. Indeed, it is likely that all of the sources were involved in either triggering or sustaining carbon emission during the PETM.

The quantities of carbon added during the PETM span the estimates of current fossil-fuel resources, suggesting that the PETM could serve as a good analogue for future warming. However, the peak rates of PETM carbon addition in these simulations (also see refs 9, 15 and 25), and in complementary simulations based on other published isotope records, are a small fraction of the present rate of fossil-fuel burning. Thus, although the current overall capacity for society to perturb the carbon cycle is comparable to that of the PETM, the rate at which we are imposing the current perturbation on the Earth system may be unprecedented.

Methods

Geochemistry. Samples weighing between 10 and 30 g were collected every ~30 cm from 554.72 to 500 mbs and every 1 m from 500 to 475 mbs from core BH9-05 for a total of 172 across the PETM. All samples were gently washed with deionized distilled water (DDW) to remove any surface contamination before extraction. 5–10 g samples were crushed in a vanadium carbide ball mill using a SPEX 8000 Mixer, resulting in a homogeneous powdered sample (size ~75 µm). The grinding jar was cleaned between samples with DDW. To remove carbonate material (siderite was present in many samples), powdered samples were reacted with 10% HCl (w/v) in centrifuge tubes for 24 h and rinsed with DDW repeatedly until pH was ~6. Samples were then freeze-dried for isotope analysis. Isotopic analyses and weight per cent data for nitrogen and carbon were carried out by continuous flow on an elemental analyser (EA; COSTECH ECS4010) coupled to an isotope ratio mass spectrometer (IRMS; Thermo Finnegan Delta Plus XP), through an open-split interface. All analyses were performed in the Stable Isotope Biogeochemistry Lab at the Pennsylvania State University. Data are reported using delta notation relative to atmospheric N_2 for nitrogen and the Vienna Pee Dee Belemnite International Standard (V-PDB) for carbon. Reference gases were calibrated relative to standards IAEA N1, N2 and N3 for nitrogen and ANU sucrose for carbon in combination with in-house, Devonian black shale, caffeine and Peru mud isotopic standards for nitrogen and carbon. Standard precision was often better than ±0.15‰ for N, but is reported as ±0.2‰ to reflect reported precision from known isotopic values of IAEA nitrogen standards. Carbon isotope values were normalized to the V-PDB scale using laboratory standards (calibrated with IAEA standards) and a two-point calibration following the methods of Coplen and colleagues[30]. Precision for C was monitored with standards across all EA analyses and was determined to be 0.21‰ ($n = 266$, 1σ). Accuracy for C was determined by measuring the difference between expected and measured values of standards treated as samples across all EA analyses and was 0.18‰ ($n = 105$). Carbon and nitrogen isotopic peak heights were calibrated to acetanilide (Costech) and Devonian black shale and Peru Mud standard of known elemental composition with a standard error of ±0.1 wt% for carbon and ±0.05 wt% for nitrogen. C/N values are reported as atomic ratios.

Carbon cycle modelling. An Earth system model of intermediate complexity (EMIC, GENIE-1: Grid ENabled Integrated Earth system model; http://www.genie.ac.uk) was used to constrain the rate and cumulative amount of carbon release necessary to generate both the magnitude and the shape of the observed PETM isotopic record and deep-sea sedimentary response[31,32]. Several of the model parameters used here were those selected by Panchuk *et al.*[25] to give the best fit to the pre-PETM observations and consistency with published estimates of Palaeocene/Eocene seawater chemistry. These include the specified detrital flux (non-carbonate) to the sediments (0.18 g cm^{-2} kyr^{-1}), the rain ratio of $CaCO_3$/POC(0.2), the global average concentrations of Ca^{2+} and Mg^{2+} (18.2 and 29.9 mmol kg^{-1}, respectively), the early Eocene palaeobathymetry and continental configuration of Bice *et al.*[33] (Supplementary Fig. S14), and a solar constant reduced 0.46% relative to modern. We selected a late Palaeocene atmospheric pCO_2 initial condition of 3× the pre-industrial level (834 µatm), which gives a deep sea temperature (10 °C) close to the benthic-foraminifera-derived temperature[34] and well within the rather large range of estimates of 300 to >2,000 µatm of late Palaeocene atmospheric pCO_2 based on modelling and many proxy studies[3,4,35–39]. To initiate the simulations, we first spun up the model for 20,000 yr as a closed system, without weathering input and sediment output but forced to equilibrate with an atmospheric pCO_2 of 834 µatm and $\delta^{13}C$ of −6.5‰, which is within the range of estimates based on $\delta^{13}C_{atm}$ reconstructions[40]. We then performed an open-system spin-up of 30,000 model years with riverine input chosen to balance the sediment output consistent with the closed system run. The model was initiated with two different river bicarbonate fluxes (9 and 32 Tmol yr^{-1}) that generate two contrasting seafloor carbonate distributions (which we refer to as 'shallow CCD' and 'deep CCD' initial conditions). Our palaeobathymetry is based on the reconstruction of Bice *et al.*[33], which is coarse in resolution and in need of revision (Supplementary Fig. S14). Many key locations are poorly represented in the model bathymetry. We address this issue as Panchuk *et al.*[25] did, by plotting the observed and modelled distribution of $CaCO_3$ with depth for large regions of the ocean that are well represented by data, including the central Pacific Ocean, Walvis Ridge (South Atlantic Ocean) and the South Indian Ocean/Southern Ocean. The approach is congruent with the way in which lysoclines and CCDs are determined based on modern sediment compositions[41].

Received 26 February 2011; accepted 12 May 2011; published online 5 June 2011

References

1. Röhl, U., Westerhold, T., Bralower, T. J. & Zachos, J. C. On the duration of the Paleocene–Eocene Thermal Maximum (PETM). *Geochem. Geophys. Geosyst.* **8,** Q12002 (2007).
2. Charles, A. J. *et al.* Constraints on the numerical age of the Paleocene–Eocene boundary. *Geochem. Geophys. Geosyst.* doi:10.1029/2010GC003426 (in the press).

3. Sluijs, A. *et al.* Subtropical Arctic Ocean temperatures during the Palaeocene/Eocene Thermal Maximum. *Nature* **441,** 610–613 (2006).
4. Zachos, J. C. *et al.* A transient rise in tropical sea surface temperature during the Paleocene–Eocene Thermal Maximum. *Science* **302,** 1551–1554 (2003).
5. Pagani, M., Caldeira, K., Archer, D. & Zachos, J. C. An ancient carbon mystery. *Science* **314,** 1556–1557 (2006).
6. Zachos, J. C. *et al.* Rapid acidification of the ocean during the Paleocene–Eocene Thermal Maximum. *Science* **308,** 1611–1615 (2005).
7. Colosimo, A., Bralower, T. & Zachos, J. *Proceedings of the Ocean Drilling Program, Scientific Results* Vol. 198 (2006).
8. Dickens, G. R., O'Neil, J. R., Rea, D. K. & Owen, R. M. Dissociation of oceanic methane hydrate as a cause of the carbon isotope excursion at the end of the Paleocene. *Paleoceanography* **10,** 965–971 (1995).
9. Zeebe, R. E., Zachos, J. C. & Dickens, G. R. Carbon dioxide forcing alone insufficient to explain Palaeocene–Eocene Thermal Maximum warming. *Nature Geosci.* **2,** 576–580 (2009).
10. Kurtz, A. C., Kump, L. R., Arthur, M. A., Zachos, J. C. & Paytan, A. Early Cenozoic decoupling of the global carbon and sulfur cycles. *Paleoceanography* **18,** 1090 (2003).
11. Higgins, J. & Schrag, D. Beyond methane: Towards a theory for the Paleocene–Eocene Thermal Maximum. *Earth Planet. Sci. Lett.* **245,** 523–537 (2006).
12. Svensen, H. *et al.* Release of methane from a volcanic basin as a mechanism for initial Eocene global warming. *Nature* **429,** 542–545 (2004).
13. Kelly, D. C., Nielsen, T. M. J., McCarren, H. K., Zachos, J. C. & Röhl, U. Spatiotemporal patterns of carbonate sedimentation in the South Atlantic: Implications for carbon cycling during the Paleocene–Eocene thermal maximum. *Palaeogeogr. Palaeoclimatol. Palaeoecol.* **293,** 30–40 (2010).
14. Walker, J. & Kasting, J. Effects of fuel and forest conservation on future levels of atmospheric carbon dioxide. *Palaeogeogr. Palaeoclimatol. Palaeoecol.* **97,** 151–189 (1992).
15. Dickens, G. R., Castillo, M. M. & Walker, J. C. G. A blast of gas in the latest Paleocene; simulating first-order effects of massive dissociation of oceanic methane hydrate. *Geology* **25,** 259–262 (1997).
16. Uroza, C. A. & Steel, R. J. A highstand shelf-margin delta system from the Eocene of West Spitsbergen, Norway. *Sedim. Geol.* **203,** 229–245 (2008).
17. Bruhn, R. & Steel, R. High-resolution sequence stratigraphy of a clastic foredeep succession (Paleocene, Spitsbergen): An example of peripheral-bulge-controlled depositional architecture. *J. Sedim. Res.* **73,** 745–755 (2003).
18. Riber, L. *Paleogene Depositional Conditions and Climatic Changes of the Frysjaodden Formation in Central Spitsbergen (Sedimentology and Mineralogy)* Unpublished Master thesis, Univ. Oslo (2009), p. 112.
19. Dypvik, H. *et al.* The Paleocene–Eocene Thermal Maximum (PETM) in Svalbard—clay mineral and geochemical signals. *Palaeogeogr. Palaeoclimatol. Palaeoecol.* **302,** 156–169 (2011).
20. Harding, I. C. *et al.* Sea-level and salinity fluctuations during the Paleocene–Eocene Thermal Maximum in Arctic Spitsbergen. *Earth Planet. Sci. Lett.* **303,** 97–107 (2011).
21. Hughes, W., Holba, A. & Dzou, L. The ratios of dibenzothiophene to phenanthrene and pristane to phytane as indicators of depositional environment and lithology of petroleum source rocks. *Geochim. Cosmochim. Acta* **59,** 3581–3598 (1995).
22. Didyk, B. M., Simoneit, B. R. T., Brassell, S. C. & Eglinton, G. Organic geochemical indicators of palaeoenvironmental conditions of sedimentation. *Nature* **272,** 216–222 (1978).
23. Leithold, E. L., Blair, N. E. & Perkey, D. W. Geomorphologic controls on the age of particulate organic carbon from small mountainous and upland rivers. *Glob. Biogeochem. Cycles* **20,** GB3022 (2006).
24. Helland-Hansen, W. Sedimentation in Paleogene foreland basin, Spitsbergen. *AAPG Bull.* **74,** 260–272 (1990).
25. Panchuk, K., Ridgwell, A. & Kump, L. R. Sedimentary response to Paleocene–Eocene Thermal Maximum carbon release: A model-data comparison. *Geology* **36,** 315–318 (2008).
26. Robinson, S. A. Shallow-water carbonate record of the Paleocene–Eocene Thermal Maximum from a Pacific Ocean guyot. *Geology* **39,** 51–54 (2011).
27. Le Quéré, C. *et al.* Trends in the sources and sinks of carbon dioxide. *Nature Geosci.* **2,** 831–836 (2009).
28. Bowen, G. J. & Zachos, J. C. Rapid carbon sequestration at the termination of the Palaeocene–Eocene Thermal Maximum. *Nature Geosci.* **3,** 866–869 (2010).
29. Svensen, H., Planke, S. & Corfu, F. Zircon dating ties NE Atlantic sill emplacement to initial Eocene global warming. *J. Geol. Soc.* **167,** 433–436 (2010).
30. Coplen, T. B. *et al.* New guidelines for ^{13}C measurements. *Anal. Chem.* **78,** 2439–2441 (2006).
31. Ridgwell, A. Interpreting transient carbonate compensation depth changes by marine sediment core modeling. *Paleoceanography* **22,** PA4102 (2007).
32. Ridgwell, A. & Hargreaves, J. C. Regulation of atmospheric CO_2 by deep-sea sediments in an Earth system model. *Glob. Biogeochem. Cycles* **21,** GB2008 (2007).
33. Bice, K. L., Barron, E. J. & Peterson, W. H. in *Tectonic Boundary Conditions for Climate Reconstructions* (eds Crowley, T. & Burke, K.) 227–247 (Oxford Univ. Press, 1998).
34. Zachos, J. C. Trends, rhythms, and aberrations in global climate 65 Myr to present. *Science* **292,** 686–693 (2001).
35. Berner, R. A. A model for atmospheric CO_2 over Phanerozoic time. *Am. J. Sci.* **291,** 339–376 (1991).
36. Cerling, T. Carbon dioxide in the atmosphere: Evidence from Cenozoic and Mesozoic paleosols. *Am. J. Sci.* **291,** 377–400 (1991).
37. Koch, P., Zachos, J. & Gingerich, P. Correlation between isotope records in marine and continental carbon reservoirs near the Paleocene/Eocene boundary. *Nature* **358,** 319–322 (1992).
38. Shellito, C., Sloan, L. & Huber, M. Climate model sensitivity to atmospheric CO_2 levels in the Early–Middle Paleogene. *Palaeogeogr. Palaeoclimatol. Palaeoecol.* **193,** 113–123 (2003).
39. Pagani, M., Zachos, J., Freeman, K., Tipple, B. & Bohaty, S. Marked decline in atmospheric carbon dioxide concentrations during the Paleogene. *Science* **309,** 600–603 (2005).
40. Smith, F., Wing, S. & Freeman, K. Magnitude of the carbon isotope excursion at the Paleocene–Eocene Thermal Maximum: The role of plant community change. *Earth Planet. Sci. Lett.* **262,** 50–65 (2007).
41. Broecker, W. & Peng, T. *Tracers in the Sea* (Eldigio, 1982).

Acknowledgements

We thank J. Zachos, T. Bralower, T. White, M. Arthur, D. Bice, G. Dickens, R. Zeebe, A. Sluijs and G. Bowen for discussions, and D. Walizer for assistance in the laboratory. High resolution core sampling by J. Nagy, H. Dypvik, L. Riber, D. Jargvoll and M. Jochmann is appreciated. This research was supported by The Worldwide Universities Network, Pennsylvania State University, US National Science Foundation awards EAR-0628486 and EAR-06520020 to L.R.K. and EAR-0844 212 to K.H.F.

Author contributions

L.R.K., Y.C. and A.J.R. designed the research. Y.C. carried out all the model simulations. Y.C., C.K.J. and A.F.D. conducted geochemical analyses. Y.C. and L.R.K. wrote the paper with contributions from A.J.C., C.K.J. and A.F.D. All authors contributed to interpretation of data.

Additional information

The authors declare no competing financial interests. Supplementary information accompanies this paper on www.nature.com/naturegeoscience. Reprints and permissions information is available online at http://www.nature.com/reprints. Correspondence and requests for materials should be addressed to Y.C.